



Cite this: *RSC Adv.*, 2017, 7, 6013

Chemical manipulation of edge-contact and encapsulated graphene by dissociated hydrogen adsorption

S. J. Hong,^{†a} H. Kim,^b M. Lee,^c H. Kang,^a M. Park,^a D. H. Jeong,^c S. W. Lee,^d Y. W. Park^{*a} and B. H. Kim^{*e}

Due to its important role in the mass production of electronics, chemical functionalization is commonly utilized during the development of graphene-based electronics. Dramatically improved graphene devices with encapsulated edge-contact configurations represent an additional application of a suitable functionalization process. In this study, we report the partial functionalization of a novel device by dissociative hydrogen adsorption. We investigate the H₂ adsorption process, which results in a change in the electrical properties using an encapsulated edge-contact device. When using chemical functionalization, we found that hydrogenation allows the realization of high-quality two-dimensional material-based electronics.

Received 15th November 2016
Accepted 10th January 2017

DOI: 10.1039/c6ra26853f

www.rsc.org/advances

1. Introduction

The van der Waals (vdW) heterostructure has been extensively studied because several viable combinations of two-dimensional (2D) materials are expected to be able to contribute to improving different electronic properties.¹ A prototypical example is the graphene and hexagonal boron nitride (h-BN) heterostructure to realize a high-mobility device.² h-BN, characterized by a smooth surface, the absence of dangling bonds, and an atomic lattice structure similar to that of graphene, is suitable for use as the basic building block of the graphene-based vdW heterostructure. h-BN has also been utilized for the encapsulation of graphene (*e.g.* h-BN/graphene/h-BN) to prevent its degradation due to exposure to ambient conditions. Indeed, it has been reported that encapsulation contributes to the electrical stability of graphene devices.^{3,4} The encapsulated configuration can be extended to other 2D materials which are extremely sensitive to air as well.⁵

Furthermore, the encapsulated configuration has introduced the novel concept of electrical contact to form an atomic contact of carbon to a metal electrode.⁶ As a result, the electronic performance has been enhanced to its theoretical limits.

Wang *et al.* reported that the mobility of graphene reached 140 000 cm² V⁻¹ s⁻¹ at room temperature.⁶ The maximum mean free path (MFP) is linearly dependent on the size of the device up to 15 μm. This indicates that the MFP has not reached its intrinsic impurity-limited scattering length. Furthermore, the contact resistance, *i.e.*, an interruption in high-performance electronic devices, was reduced to 150 Ω μm. Owing to these advantages, the encapsulated configuration is expected to be a prototype of a high-quality 2D electronic device. In order to develop this novel concept of an electronic device to the point of application, chemical manipulation may be feasible due to its compatibility with mass-production. In this regard, the tight interface of the vdW heterostructure³ must be overcome. Therefore, it is necessary to explore the intercalation, adsorption, and doping of molecules in h-BN/graphene/h-BN devices so as to make chemical manipulation a viable approach.

Hydrogen is an attractive element to functionalize carbon atom, as it yields stable chemical C–H bonds. With different approaches, various electronic properties have been observed in graphene-based materials modified by hydrogen.^{7–10} For example, the hydrogenation of graphene-based materials results in a metal–insulator transition,⁷ electron doping,^{8,9} and the realization of atomic magnets in local regions.¹⁰ The hydrogenation has been applied for improvement of graphene device. At first, the studies were performed on bare SiO₂ substrate.^{7–9} With the help of the h-BN substrate, the hydrogenation has been applied to high-quality graphene device and revealed its intrinsic effects on graphene.¹¹ For ultimate device configuration, h-BN/graphene/h-BN, few researches have been achieved and it is even unclear whether hydrogen molecules can be intercalated or not. Meanwhile, the recent report in which a high-pressure H₂ environment has shown the successful

^aDepartment of Physics and Astronomy, Seoul National University, Seoul 08826, Korea. E-mail: ywpark@snu.ac.kr

^bKorea Research Institute of Standards and Science (KRISS), Daejeon 34113, Korea

^cDepartment of Chemistry Education, Seoul National University, Seoul 08826, Korea

^dDepartment of Physics, Ewha Womans University, Seoul, 03760, Korea

^eDepartment of Physics, Incheon National University, Incheon 22012, Korea. E-mail: kbh37@inu.ac.kr

[†] Present address: Institut für Festkörperphysik, Leibniz Universität Hannover, Appelstraße 2, 30167, Hannover, Germany.



intercalation of molecules between graphene layers in graphite¹² provides the evidence of the feasibility of chemical manipulation in the vdW structure of h-BN/graphene/h-BN.

Here, we investigate the hydrogenation in the h-BN/graphene/h-BN heterostructure and report the successful intercalation and modification of electrical properties. A vdW heterostructure was fabricated using chemical vapor deposition (CVD)-grown single-layer graphene (SLG) with exfoliated h-BN flakes, yielding a high-quality edge-contact configuration. The intercalation and adsorption of dissociative hydrogen in the vdW structure were revealed by Raman spectroscopy. The adsorption met the requirements of the first-order adsorption model and resulted in electron doping, short-range scattering, and a reduction of the contact resistance. Furthermore, we confirmed the maintenance of these properties even under a high vacuum environment. The hydrogenation of an edge-contact graphene device is expected to contribute to the realization of the chemical manipulation of high-quality graphene-based electronics for mass production.

2. Experimental

SLG was grown by the CVD method¹³ and h-BN was exfoliated from a commercial crystal component (HQ graphene). We used a wet etching transfer method with a 0.1 M NaOH solution to form the h-BN/SLG/h-BN heterostructure. Thereafter, a conventional lithography process was carried out with bubble and wrinkle-free regions. Raman spectroscopy was also utilized with a 532 nm-wavelength laser, and three-terminal electrical measurements were carried out using a Keithley 4200-SCS parameter analyzer. We obtained a pristine encapsulated device which was annealed at 380 K under 5×10^{-6} Torr for 10 h in a custom-made high-pressure chamber. After annealing, *in situ* electrical measurements were taken at 350 K under H₂ (99.9999%) at 11 bar of pressure.

3. Results and discussion

The CVD-grown SLG was transferred onto the exfoliated h-BN flake on SiO₂/Si substrate by the bubbling transfer method.¹⁴ The SLG and h-BN are depicted by the white and orange dashed lines, respectively, in Fig. 1(a). Another h-BN flake depicted by the orange dashed line in Fig. 1(b) was transferred onto the SLG/h-BN, yielding the h-BN/SLG/h-BN heterostructure, as shown in Fig. 1(c). Using reactive ion etching (R.I.E.) with a mixture of O₂ and CF₄, we designed the rectangular heterostructure depicted by the red dashed line in Fig. 1(c). Finally, the edge contact was created by conventional electron beam lithography and metal evaporation (Cr/Au = 3/50 nm), as shown in Fig. 1(d). Fig. 1(e) and (f) indicate a schematic and an atomic force microscopy (AFM) image of the edge-contact device, respectively.

The Raman spectra of the center and edge regions, designated by the red and orange dots in Fig. 2(a), are presented in Fig. 2(b) and (c), respectively. We observed typical h-BN (~ 1366 cm⁻¹), G (~ 1580 cm⁻¹), and 2D (~ 2700 cm⁻¹) peaks in the center region. In the edge region, D (~ 1350 cm⁻¹) and D' (~ 1620 cm⁻¹) were also measured and found to be consistent with defective edge properties. While the G peaks scarcely changed, the 2D peaks showed a red-shift in both cases. The red-shift is understood to stem from electron doping.¹⁵ Pronounced red-shift is observed at the edge ($\Delta\omega_{2D} = 4.6$ cm⁻¹) compared to that in the center region ($\Delta\omega_{2D} = 3.5$ cm⁻¹). This finding is in good agreement with the fact that dissociative hydrogen adsorption is more active at defective sites.⁹ It is interesting that dissociative hydrogen can be intercalated through the vdW heterostructure. The intercalation of dissociated hydrogen in the vdW heterostructure is consistent with its behavior in graphite.¹² The authors reported that hydrogen at a high pressure (20 bar) can be dissociated and intercalated between graphene layers, exhibiting a reduction of the electrical conductivity on the *c*-axis. On the other hand, it has been

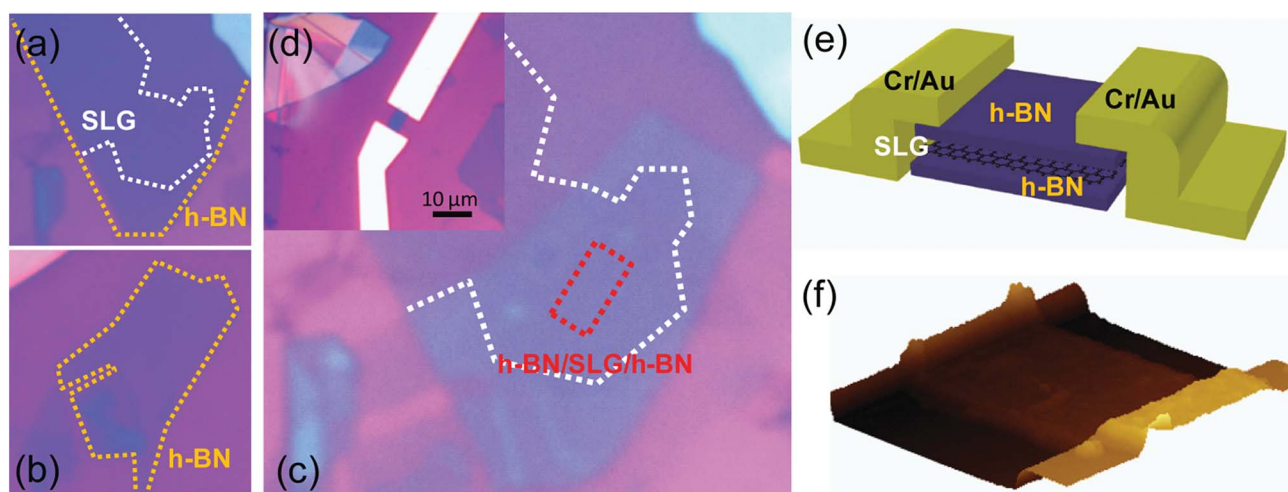


Fig. 1 Encapsulated edge-contact vdW heterostructure fabrication process. Optical image of (a) CVD-grown SLG on h-BN flake (b) h-BN flake for covering SLG/h-BN (c) h-BN/SLG/h-BN heterostructure (d) as-fabricated device, respectively. (e) and (f) indicate schematic and AFM image, respectively.



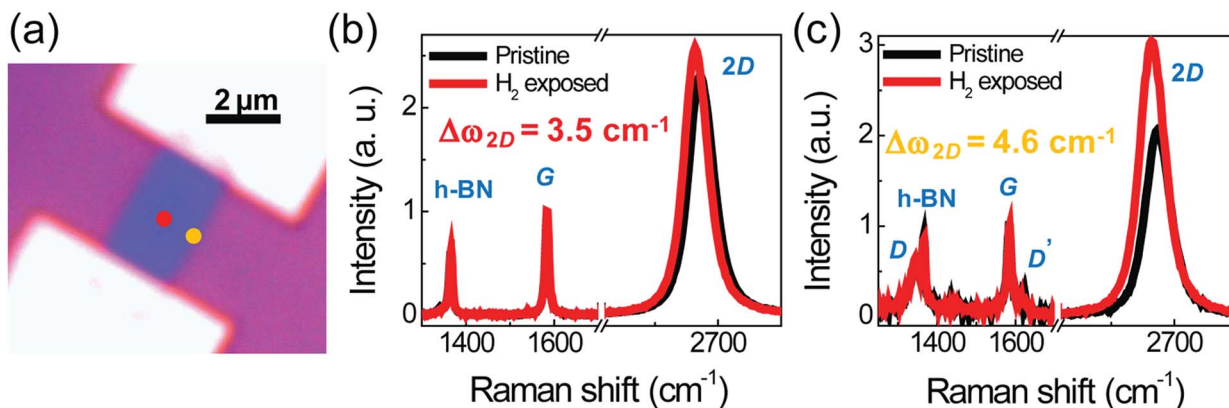


Fig. 2 (a) Optical image of encapsulated edge-contact device where red and orange dot indicate measurement position of Raman spectroscopy. Raman spectra of h-BN/SLG/h-BN in the region of (b) center and (c) edge, respectively. Black and red curves are pristine and hydrogen treated, respectively.

reported that the encapsulated structure provides tight sealing of the molecules (Br_2)¹⁶ and reduces environmental effect.³ Therefore, dissociated hydrogen can be a key factor in the chemical manipulation of encapsulated graphene devices.

Fig. 3 shows the results of an electrical analysis of the hydrogenation of the h-BN/SLG/h-BN heterostructure. The edge-contact device shows typical transfer characteristics (R vs. V_g), as shown in Fig. 3(a). The transfer curve moved to negative gate voltage (V_g) side, indicating an electron doping effect. We undertook fitting to the transfer curve model of SLG,¹⁷

$$R_{\text{total}} = 2R_c + R_{\text{sample}} = 2R_c + \frac{1}{e\mu} \left(\frac{L}{W} \right) \frac{1}{\sqrt{n^2 + n_0^2}}, \text{ where } R_c, e, \mu,$$

L (W), n and n_0 are the contact resistance, the charge element, the mobility, the length (width) of the sample, the carrier density and the residual carrier density, respectively. We used the carrier density relationship with a parallel conductor model, $n = \alpha(V_g - V_D)$, where V_D corresponds to the Dirac point and $\alpha_{\text{SiO}_2(285 \text{ nm})} = 7.5 \times 10^{10} \text{ cm}^{-2} \text{ V}^{-1}$. It should be noted that the fittings were performed in the electron branch owing to the high asymmetry in the hole branch. The asymmetry is in agreement with the two-terminal graphene edge contact with lower work function metal, Cr electrode.⁶

In Fig. 3(b), the temporal evolution of $-\Delta V_D$ shows the first-order Langmuir type adsorption process, for which $-\Delta V_D =$

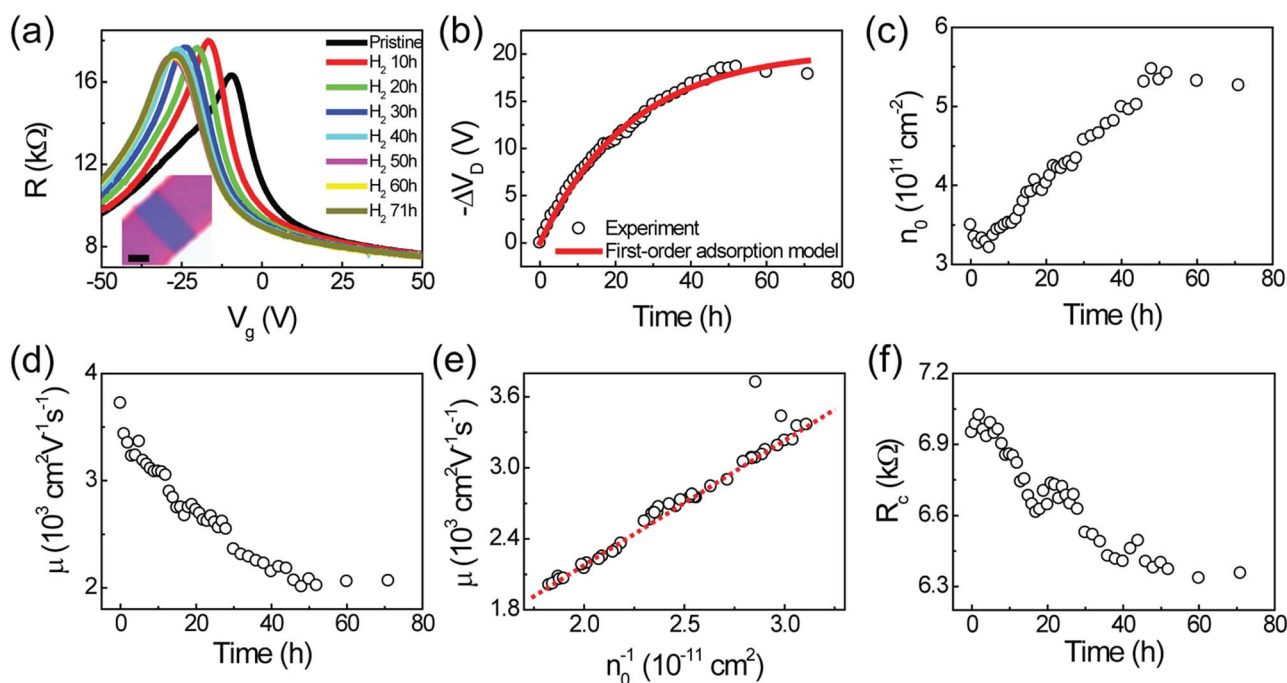


Fig. 3 *In situ* electrical monitoring of h-BN/SLG/h-BN device. (a) Transfer characteristics (R vs. V_g) with hydrogen adsorption time. Inset is optical image of the device where scale bar is $2 \mu\text{m}$. (b–d) Temporal evolution of $-\Delta V_D$, n_0 , and μ , respectively. (e) μ vs. n_0^{-1} plot where red dashed line is guide for eye. (f) Temporal evolution of R_c .



$-\Delta V_D^{\text{Sat}} (1 - e^{-kt})$, where $-\Delta V_D^{\text{Sat}}$ and k denote the saturated V_D and the kinetic coefficient, respectively. The experimental data (black circles) and the fitting function (red curve) yield the fitting parameters $-\Delta V_D^{\text{Sat}} = 20$ V and $k = 0.04$ h⁻¹, respectively. This type of first-order adsorption has been observed in different cases of molecule adsorption in graphene-based systems.^{11,18,19} The fitting parameters are very close to previous results¹¹ in which Bernal stacked bilayer graphene (BLG) on h-BN was exposed to hydrogen at both the surface and edge regions. This similar adsorption tendency indicates that hydrogen is adsorbed on the surface of h-BN/SLG/h-BN, which is consistent with the Raman spectroscopy results.

Fig. 3(c) and (d) indicate the temporal evolution of the residual density (n_0) and the mobility (μ), respectively. As hydrogen is adsorbed, n_0 increases and μ decreases due to the formation of C–H bonding. We also observed competitive behavior between n_0 and the μ (Fig. 3(c) and (d)) and short-range scattering behavior ($\mu \propto n_0^{-1}$) (Fig. 3(e)), as shown in a previous report.¹¹

The edge-contact device provides an ideal contact configuration of 2D materials. Wang *et al.* reported a novel one-dimensional contact geometry, leading to ideal contact performance and effect of chemical termination.⁶ The authors argued that the low contact resistance stems from the shorter bonding distance with larger orbital overlap in the edge-contact geometry. Furthermore, it has been discussed that oxygen termination can improve the contact performance. Note that our R_c is relatively high (~ 7 k Ω for pristine) compared to that of devices in a previous study,⁶ even when using an identical metal electrode (Cr/Au). This may originate from unintentional fluorine termination during the O₂/CF₄ plasma etching process.²⁰ We focus on the temporal evolution of R_c , which resembles the behavior of $-\Delta V_D$. In contrast to the Cr–H–graphene edge-contact configuration,²⁰ R_c was reduced due to hydrogen adsorption (Fig. 3(f)). The absence of a metal electrode effect was previously discussed with the thermoelectric power (TEP) measurements in our previous report.²¹ The reduction of R_c can be understood by the variation of density of state after hydrogen adsorption. With electron doping, the density of state in graphene increases, yielding a lower value of R_c . Recently, a similar result using poly(4-vinylphenol)/poly(melamine-co-formaldehyde) (PVP/PMF) was reported²² in which the authors observed a reduction of R_c with the concentration of PVP/PMF. In this regard, even though the direct observation of atomic termination is necessary for future work, we may conclude that the reduction of R_c is from the doping of graphene sheet but not from the chemical termination between Cr and graphene edge. Since the temporal evolution of R_c was provided by *in situ* monitoring, fine manipulation of R_c could be achieved during hydrogen adsorption.

Finally, we confirmed the stability of C–H bonding by evacuating down to 6×10^{-6} Torr, as shown in Fig. 4. The transfer curves for high-pressure H₂ (11 bar), low-pressure H₂ (1 bar), and a vacuum (6×10^{-6} Torr) condition did not show any distinctive changes, indicating strong binding of the C–H bonds. Due to the strong binding, dissociative induced hydrogen adsorption can provide a means of stable chemical functionalization.

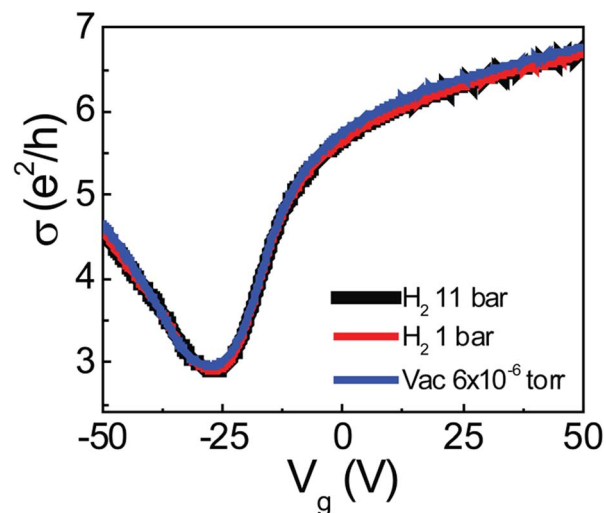


Fig. 4 Transfer characteristics (σ vs. V_g) with 11 bar, 1 bar of H₂ gas molecules, and vacuum (6×10^{-6} Torr).

4. Conclusions

In summary, we studied hydrogenation in the vdW heterostructure, which provides an encapsulated type of edge-contact geometry for CVD-grown SLG. Raman spectroscopy and electrical measurements showed the intercalation and adsorption of dissociated hydrogen. The *in situ* monitoring of the electrical properties revealed first-order adsorption, electron doping, short-range scattering, and reduced contact resistance. The electrical modulation is in good agreement with previous results with an ordinary device configuration. Specifically, considering the contact edge configuration, it was found that hydrogenation intrinsically affects graphene sheets rather than the atomic contact termination. Furthermore, strong C–H binding even under a high vacuum provides evidence of the stability of the hydrogenation process. The chemical manipulation of an encapsulated edge-contact device with the vdW heterostructure will contribute to the realization of high-quality 2D material-based electronic devices.

Acknowledgements

This work was supported by the Swedish-Korean Basic Research Cooperative Program (No. 2014R1A2A1A12067266) of the NRF and by the FPRD of BK21 plus through the MEST, Korea. Partial support was provided by Leading Foreign Research Institute Recruitment Program through the National Research Foundation of Korea (NRF) funded by the Ministry of Science, ICT & Future Planning (2015K1A4A3047345). M. L. and D. H. J. acknowledge the support of the Pioneer Research Center Program through the NRF of Korea, funded by the Ministry of Science, ICT & Future Planning (No. 2013-006163). S. W. L. acknowledges the support of National Research Foundation of Korea (NRF-2015R1A2A2A05050829). B. H. K. acknowledges the support from the National Research Foundation of Korea (No. NRF-2014R1A1A1002467).



Notes and references

- 1 A. K. Geim and I. V. Grigorieva, *Nature*, 2013, **499**, 419.
- 2 C. R. Dean, A. F. Young, I. Meric, C. Lee, L. Wang, S. Sorgenfrei, K. Watanabe, T. Taniguchi, P. Kim, K. L. Shepard and J. Hone, *Nat. Nanotechnol.*, 2010, **5**, 722.
- 3 L. Wang, Z. Chen, C. R. Dean, T. Taniguchi, K. Watanabe, L. E. Brus and J. Hone, *ACS Nano*, 2012, **6**, 9314.
- 4 C. Melios, A. Centeno, A. Zurutuza, V. Panchal, C. E. Giusca, S. Spencer, S. R. P. Silva and O. Kazakova, *Carbon*, 2016, **103**, 273.
- 5 A. Avsar, I. J. Vera-Marun, J. Y. Tan, K. Watanabe, T. Taniguchi, A. H. Castro Neto and B. Özyilmaz, *ACS Nano*, 2015, **9**, 4138.
- 6 L. Wang, I. Meric, P. Y. Huang, Q. Gao, Y. Gao, H. Tran, T. Taniguchi, K. Watanabe, L. M. Campos, D. A. Muller, J. Guo, P. Kim, J. Hone, K. L. Shepard and C. R. Dean, *Science*, 2013, **342**, 614.
- 7 D. C. Elias, R. R. Nair, T. M. G. Mohiuddin, S. V. Morozov, P. Blake, M. P. Halsall, A. C. Ferrari, D. W. Boukhvalov, M. I. Katsnelson, A. K. Geim and K. S. Novoselov, *Science*, 2009, **323**, 610.
- 8 J. Katoch, J. H. Chen, R. Tsuchikawa, C. W. Smith, E. R. Mucciolo and M. Ishigami, *Phys. Rev. B: Condens. Matter Mater. Phys.*, 2010, **82**, 081417.
- 9 B. H. Kim, S. J. Hong, S. J. Baek, H. Y. Jeong, N. Park, M. Lee, S. W. Lee, M. Park, S. W. Chu, H. S. Shin, J. Lim, J. C. Lee, Y. Jun and Y. W. Park, *Sci. Rep.*, 2012, **2**, 690.
- 10 H. González-Herrero, J. M. Gómez-Rodríguez, P. Mallet, M. Moaied, J. José Palacios, C. Salgado, M. M. Ugeda, J.-Y. Veuillen, F. Yndurain and I. Brihuega, *Science*, 2016, **352**, 437.
- 11 S. J. Hong, H. Kang, M. Park, M. Lee, D. Soler-Delgado, D. H. Jeong, Y. W. Park and B. H. Kim, *RSC Adv.*, 2015, **5**, 103276.
- 12 J. Kim, C. H. Kwak, W. Jung, Y. S. Huh and B. H. Kim, *Phys. Chem. Chem. Phys.*, 2016, **18**, 15514.
- 13 G. H. Han, J. A. Rodriguez-Manzo, C.-W. Lee, N. J. Kybert, M. B. Lerner, Z. J. Qi, E. N. Dattoli, A. M. Rappe, M. Drndic and A. T. C. Johnson, *ACS Nano*, 2013, **7**, 10129.
- 14 L. Gao, W. Ren, H. Xu, L. Jin, Z. Wang, T. Ma, L. P. Ma, Z. Zhang, Q. Fu, L.-M. Peng, X. Bao and H.-M. Cheng, *Nat. Commun.*, 2012, **3**, 699.
- 15 A. Das, S. Pisana, B. Chakraborty, S. Piscanec, S. K. Saha, U. V. Waghmare, K. S. Novoselov, H. R. Krishnamurthy, A. K. Geim, A. C. Ferrari and A. K. Sood, *Nat. Nanotechnol.*, 2008, **3**, 210.
- 16 Z. Chen, P. Darancet, L. Wang, A. C. Crowther, Y. Gao, C. R. Dean, T. Taniguchi, K. Watanabe, J. Hone, C. A. Marianetti and L. E. Brus, *ACS Nano*, 2014, **8**, 2943.
- 17 S. Kim, J. Nah, I. Jo, D. Shahrjerdi, L. Colombo, Z. Yao, E. Tutuc and S. K. Banerjee, *Appl. Phys. Lett.*, 2009, **94**, 062107.
- 18 S. Chen, W. Cai, D. Chen, Y. Ren, X. Li, Y. Zhu, J. Kang and R. S. Ruoff, *New J. Phys.*, 2010, **12**, 125011.
- 19 I. Silvestre, E. A. de Moraes, A. O. Melo, L. C. Campos, A.-M. B. Goncalves, A. R. Cadore, A. S. Ferlauto, H. Chacham, M. S. C. Mazzoni and R. G. Lacerda, *ACS Nano*, 2013, **7**, 6597.
- 20 Q. Gao and J. Guo, *APL Mater.*, 2014, **2**, 056105.
- 21 S. J. Hong, M. Park, H. Kang, M. Lee, D. Soler-Delgado, D. S. Shin, K. H. Kim, S. Kubatkin, D. H. Jeong, Y. W. Park and B. H. Kim, *Appl. Phys. Lett.*, 2015, **106**, 142110.
- 22 H.-Y. Park, W.-S. Jung, D.-H. Kang, J. Jeon, G. Yoo, Y. Park, J. Lee, Y. H. Jang, J. Lee, S. Park, H.-Y. Yu, B. Shin, S. Lee and J.-H. Park, *Adv. Mater.*, 2016, **28**, 864.

